Applied Physics Letters

Modulating the transport property of flexible $La_{0.67}Ca_{0.33}MnO_3$ thin film by mechanical bending

Cite as: Appl. Phys. Lett. **118**, 052404 (2021); https://doi.org/10.1063/5.0024516
Submitted: 10 August 2020 • Accepted: 15 January 2021 • Published Online: 01 February 2021

Wentao Hua, Lu Lu, Lvkang Shen, et al.

Applied Physics Letters ARTICLE scitation.org/journal/apl

Modulating the transport property of flexible $La_{0.67}Ca_{0.33}MnO_3$ thin film by mechanical bending

Cite as: Appl. Phys. Lett. **118**, 052404 (2021); doi: 10.1063/5.0024516
Submitted: 10 August 2020 · Accepted: 15 January 2021 ·
Published Online: 1 February 2021

Wentao Hua,[1] Lu Lu,[2] Lvkang Shen,[2] Jing Jin,[2] He Wang,[2] Ming Liu,[2] Chunrui Ma,[1,a)] and Chun-Lin Jia[2,3]

AFFILIATIONS

[1]State Key Laboratory for Mechanical Behaviour of Materials and School of Materials Science and Engineering, Xi'an Jiaotong University, Xi'an 710049, China
[2]School of Microelectronics, Xi'an Jiaotong University, Xi'an 710049, China
[3]Ernst Ruska Centre for Microscopy and Spectroscopy with Electrons, Forschungszentrum Jülich, D-52425 Jülich, Germany

[a)]**Author to whom correspondence should be addressed:** chunrui.ma@mail.xjtu.edu.cn

ABSTRACT

Flexible epitaxial $La_{0.67}Ca_{0.33}MnO_3$ (LCMO) thin films are fabricated on an $SrTiO_3$ buffered (001)-oriented fluorophlogopite substrate. The metal-to-insulator transition tends toward lower temperature when subjected to mechanical bending. Moreover, the transport behavior of the bent LCMO films in the insulating region follows the variable range hopping model and the resistivity increases with the reduction in the bending curvature radii because the applied strain aggravates the distortion of the LCMO crystal structure, decreases the hopping distance, and, hence, impedes the transport of charge carriers. The resistivity change induced by the mechanical bending can go up to 10^4% at 100 K and 10^5% at 10 K. Such a large resistivity change makes the flexible LCMO thin film promising as a mechanical-bending switch device at low temperature.

Thin films of mixed-valence perovskite manganites $La_{1-x}A_xMnO_3$ (A = Sr, Ca, Ba) have attracted worldwide attention due to the abundant distinct physical phenomena, such as the colossal magnetoresistance effect, the transition from the paramagnetic to ferromagnetic state, the metal to insulator transition (MIT), phase separation, and so on.[1–4] These ponderable physical mechanisms make it potentially applicable in the area of magnetic random-access memories, magnetoelectric devices, tunneling magnetoresistance devices, and switching devices.[5–7] Among these materials, $La_{0.67}Ca_{0.33}MnO_3$ (LCMO) has become one of the mostly invested materials due to its complex pattern of spin, orbital, charge, and Jahn–Teller lattice distortions,[8–10] which induces a variety of exotic phenomena, such as a huge magnetoresistance effect. Moreover, as the representative of narrow bandwidth manganites with robust Jahn–Teller coupling, its electrical transport is very sensitive to the external environment and exhibits various novel physical phenomena.[11,12] A small external perturbation can influence the Mn^{3+}/Mn^{4+} exchange effect[13] and the Jahn–Teller distortion[14] and, thus, generate a large change in transport properties. So far, many researchers have devoted effort to investigate the effect of the external strain on its physical mechanism. One way was to take advantage of the lattice mismatch between the film and the substrate to build various interface strains.[15,16] For example, Helali *et al.* fabricated LCMO on $LaAlO_3$, $SrTiO_3$, and $(LaAlO_3)_{0.3}$–$(SrAlTaO_6)_{0.7}$ to generate compressive strain, tensile strain, and negligible tensile strain, respectively. It is found that both tensile and compressive strain can increase the thermal activation energy and the variable range hopping (VRH) characteristic temperature in the paramagnetic state.[17] Another way to study the strain effect on transport behavior was to fabricate several samples with different thicknesses since the interface strain induced by the lattice mismatch between the film and the substrate is gradually released by formation of dislocations or defects with the increasing film thickness.[18,19] Wang *et al.* found that a dead layer about 6 nm thick was formed in LCMO epitaxial thin films and the conductivity of the films linearly increased with the film thickness due to the reduced effects of the dead layer.[20] However, the properties of the films are affected not only by strain but also by the microstructure induced by different growth modes and by crystalline quality on different substrates. Therefore, it is necessary to find a way to explore the influences of pure strain on the film properties.

A flexible thin film not only is the basis of wearable/portable electronic devices but also provides a test sample for modulating or exploring the novel physical properties by applying stretching strain or mechanical bending strain. Until now, two methods have been used to fabricate flexible epitaxial function oxide thin films. One is to transfer

the desired thin film from a rigid substrate to a flexible substrate through etching a buffer layer between the desired thin film and the rigid substrate.[20] Another is to directly fabricate the desired thin film on a flexible mica substrate.[21] Recently, Hong *et al.* investigated the effect of extreme tensile strain on $La_{0.7}Ca_{0.3}MnO_3$ membranes fabricated through transferring the epitaxial $La_{0.7}Ca_{0.3}MnO_3$ thin film onto the polyimide sheet and found that uniaxial and biaxial tensile strain benefits the formation of the antiferromagnetic insulating state and suppression of ferromagnetic metal.[22] However, few research studies contributed to investigation of the effects of mechanical bending strain on the transport properties of the LCMO thin films. Compared to the transferring method, the direct fabrication method can effectively avoid the contamination induced during the transferring process.

In the present paper, the flexible epitaxial (111) LCMO thin films were fabricated on the $SrTiO_3$ (STO)-buffered (001) fluorophlogopite single-crystalline substrates (F-Mica). The effects of mechanical bending strain on the transport properties of the LCMO thin films were explored with and without the magnetic field.

For preparation of the flexible epitaxial LCMO thin films, an epitaxial STO buffer layer was first deposited on the (001) F-Mica substrate at an oxygen pressure of 50 mTorr via a 248 nm KrF excimer pulsed laser deposition (PLD) system with the laser energy of 500 mJ. Then, the oxygen pressure and the laser energy were increased to 250 mTorr and 650 mJ to grow the LCMO thin film on top of the STO buffer layer. The repetition rate of the laser was fixed at 5 Hz for the growth of both STO and LCMO. After deposition, the thin films were annealed at 1000 °C for 15 min at an oxygen pressure of 200 Torr and then cooled down to room temperature at a rate of 25 °C per min. The crystallinity and quality of the epitaxial LCMO thin films were characterized by high-resolution X-ray diffraction (HRXRD) using a PANalytical X'Pert MRD system. Reciprocal space mappings (RSMs) were conducted to determine the crystal structure by using a scanning line detector. The microstructure of the films was investigated by transmission electron microscopy (TEM). The transport properties were measured by the Van der Pauw method using a physical property measurement system (PPMS). The flexible film/F-Mica was peeled off mechanically from the substrate bulk with the assistance of the polyimide type. The bending states of the LCMO thin films were realized by attaching the films to an insulating double-faced adhesive tape on the copper molds with the bending curvature radii of 25 mm, 12.5 mm, and 7.5 mm.

Figure 1(a) shows the XRD θ–2θ scanning pattern of the LCMO and STO thin film system on the F-Mica substrate. Only the (111) and (222) peaks of LCMO and STO and the {00*l*} peaks of F-Mica can be seen, showing that the films grow with the {111} atomic planes parallel to the (001) plane of the F-Mica substrate. In order to investigate the in-plane orientation relationship between the film and the F-Mica substrate, φ scans were performed around {002} reflections of STO and LCMO and {202} reflections of the F-Mica substrate as shown in Fig. 1(b). It is clearly seen that the F-Mica peaks show threefold symmetry and the films exhibit a sixfold symmetry, which is indicative of the in-plane relationship of $[1\bar{1}0]_{LCMO}//[1\bar{1}0]_{STO}//[010]_{F\text{-}Mica}$. According to the out-of-plane and in-plane orientation relationship between the films and the substrates, it can be derived that the fabricated films are epitaxial. This epitaxial relationship is also confirmed by the selected-area electron diffraction (SAED) pattern of the sample recorded along the $[1\bar{1}0]$ zone axis of F-Mica, as shown in the inset of

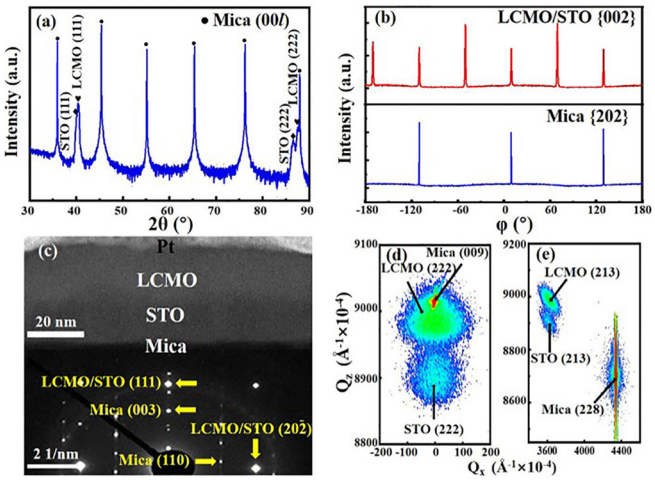

FIG. 1. (a) XRD θ–2θ pattern of the LCMO thin film and STO buffer layers on the (001) F-Mica substrate. (b) The φ scans taken around the {202} reflections of F-Mica and {002} reflections of LCMO/STO, respectively. (c) The TEM image of a cross-section of the sample and the SAED patterns taken from the areas covering the interfaces between the films and the substrate. (d) RSMs taken around the symmetric (222) of the LCMO thin film. (e) RSMs taken around asymmetric (213) reflections of the F-Mica substrate.

Fig. 1(c). The thicknesses of the LCMO and STO layers are around 22 nm and 13 nm, respectively, which were measured from the cross-sectional TEM image [Fig. 1(c)]. From the symmetric RSMs taken around the (111) reflections of the multilayer and the (001) reflection of the F-Mica substrate in Fig. 1(d), the (111) plane spacings of the LCMO and STO layers are measured to be 2.218 Å and 2.239 Å, respectively. In comparison with the corresponding (111) plane spacings (2.227 Å for LCMO and 2.255 Å for STO) of bulk materials,[23] the LCMO and STO thin films undergo compressive strains of ~0.40% and ~0.71%, respectively, along the out-of-plane direction. From the asymmetric RSMs taken around the (213) reflections of the LCMO films and the (228) reflections of the F-Mica substrates, as shown in Fig. 1(e), plane spacings of 1.884 Å and 1.887 Å are measured along the in-plane $[1\bar{1}0]$ directions, respectively, for the LCMO and STO layers, which are larger than those of the LCMO (1.819 Å) and the STO (1.841 Å) bulk materials, leading to in-plane tensile strains of ~3.57% in the LCMO layer and ~2.50% in the STO layer.

Figures 2(a) and 2(b) (linear scale shown in Figs. S2–S5) show the data of resistivity measured in a range of temperatures from 10 to 350 K at 0 T in tensile and compressive mechanical strain. A normal MIT process occurs for the film in the flat state and the transition temperature is about 204 K, which is lower than the value of bulk material (265 K), probably due to the in-plane tensile strain of 3.57% induced by the lattice mismatch between the films and the substrate.[24] The transition temperature tends to lower temperature in the mechanical bending state since the mechanical bending-induced tensile and compressive strains are likely to distort the lattices of the film and, hence, hinder the transport of charge carriers in the film, making LCMO reach the insulator state earlier when it is warmed from 10 to 350 K. This phenomenon consists of the Monte Carlo simulation reported by Sen and Dagotto that LCMO gradually reaches an insulating charge-ordered phase from a charge disordered metallic phase as strain

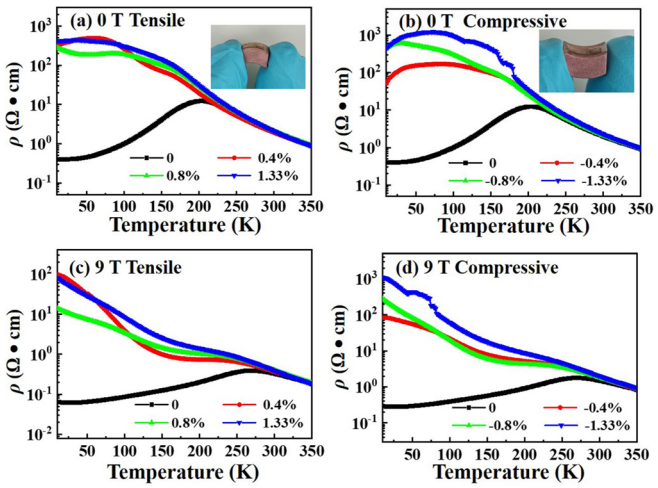

FIG. 2. Transport properties of the flexible LCMO thin film under extra mechanical tensile and compressive strain induced by convex and concave bending without the magnetic field (a) and (b) and with the 9 T magnetic field (c) and (d).

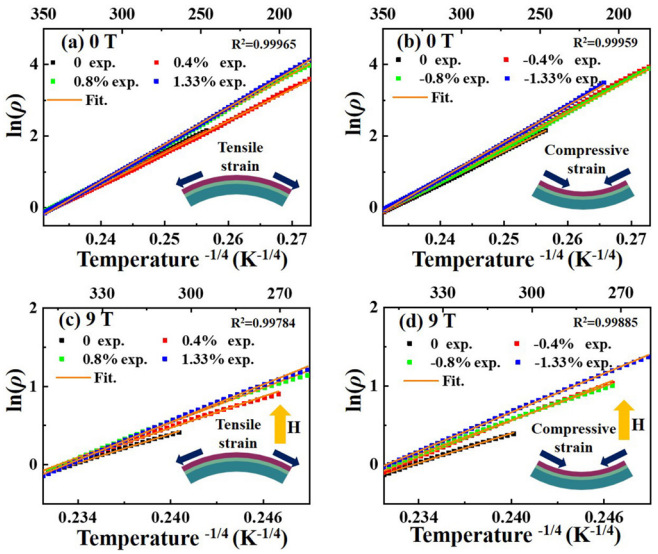

FIG. 3. Logarithm of the resistivity vs $T^{-1/4}$ plot of the LCMO thin film under extra tensile and compressive strain induced by various bending curvature radii above the transition temperature at 0 T (a) and (b) and 9 T (c) and (d).

increases.[25] From Fig. 2(c), it can be seen that the MIT temperature increases to 268 K in the flat state, indicating that the magnetic field enhances the double exchange and postpone it to enter the insulator state. However, it is unexpected that the MIT disappears in the test temperature range under the mechanical bending strain as shown in Figs. 2(c) and 2(d). The abnormal phenomena probably can contribute to the slowly decreasing resistivity with the increase in temperature. It is known that the magnetic field will provide the energy to assist charge carrier to transport in the film and reduce the resistivity of LCMO (Fig. S6), while the mechanical bending strain prevents the charge carrier to transport and increase its resistivity. The competition between energy from the magnetic field and mechanical bending strain merges MIT. In order to understand the transport mechanism under the effect of extra mechanical strain, the measured resistivity in the high temperature region was simulated using the thermal activation model (Fig. S7),[23] small-polaron hopping (Fig. S8),[26] and VRH model.[27] It is found that the VRH model fits the data very well, as shown in Fig. 3, implying that the transport mechanism in the LCMO films is the charge carrier hopping between localized electronic states.

In the VRH model, $\rho(T) = \rho_0 e^{(T_0/T)^{1/4}}$, where T_0 represents the characteristic temperature and is proportional to the slope of a plot of $\ln(\rho)$ vs $T^{-1/4}$.[27] It is known that the average nearest-neighbor hopping distance $R = \left[\frac{9}{8\pi\alpha N(E)kT}\right]^{1/4}$ and the localization length $\frac{1}{\alpha} = \left(\frac{171U_mV}{kT_0}\right)^{1/3}$, where V is the unit-cell volume per Mn ion, k is the Boltzmann constant, and $U_m = 3J_H/2$ is the splitting energy between the spin-up and spin-down e_g bands. J_H is the coefficient of Hund's rule coupling, and $U_m \approx 2$ eV in manganites. $N(E)$ is the available density of states, where the charge carrier can hop to. Based on the calculation of Viret *et al.*, the $N(E)$ value is around 9×10^{26} m^{-3} eV^{-1}.[26] Here, we assume the volume of unit-cell conservation under the strain. Hence, the hopping distance can be obtained and is summarized in Table I with the fit value of T_0. It is found that the hopping distance decreases with the increase in mechanical bending strain, no matter tensile or compressive strain, except the compressive strain of 0.8%, which is slightly larger than the value of the compressive strain of 0.4%. T_0 exhibits an opposite trend to the hopping distance. It is known that T_0 is proportional to the hopping energy from one

TABLE I. The VRH characteristic temperature and average nearest-neighbor hopping distance R of different tensile or compressive strains derived from the resistivity of LCMO as a function of temperature at 0 T and 9 T.

	Tensile				Compressive			
	0 T		9 T		0 T		9 T	
$\rho = \rho_0 \times e^{(\frac{T_0}{T})^{\frac{1}{4}}}$ Strain	T_0 (10^7 K)	R (Å)	T_0 (10^7 K)	R (Å)	T_0 (10^7 K)	R (Å)	T_0 (10^7 K)	R (Å)
0	6.82	12.30	1.4	14.03	6.82	12.30	1.4	14.03
0.4%	7.23	12.24	1.76	13.77	9.33	11.98	3.3	13.07
0.8%	9.47	11.96	2.57	13.34	9.08	12.02	2.46	13.39
1.33%	10.63	11.84	3.63	12.97	12.91	11.65	4.28	12.79

localized state to another.[28,29] The reduction in the hopping distance and the increased hopping energy indicate that the applied strain aggravates the distortion of the LCMO crystal structure and impedes the transport of the charge carrier and enhance its insulator behavior.[22]

Figure 4 exhibits the resistivity change ratio $(\rho_{bent} - \rho_{flat})/\rho_{flat} \times 100\%$, where ρ_{bent} and ρ_{flat} are the resistivity of the film in the bending and flat state, as a function of temperature from 10 to 200 K with and without the magnetic field. It is found that the resistivity change ratio increases from $\sim 10^2\%$ at 200 K to $\sim 10^4\%$ at 100 K and then it slowly increases to $\sim 10^5\%$ at 50 K and almost remains unchanged until 10 K. The change ratio is even higher with the application of a magnetic field. As shown in Fig. 2, the huge resistivity change without/with the magnetic field can contribute to the different scenario of $\rho(T)$ at low temperature. The LCMO thin film remains in a metallic state in the absence of extra mechanical strain, while the application of mechanical strain triggers an insulating state. As the calculation by Sen and Dagotto is based on Monte Carlo simulation, there is a transition in the LCMO from a metallic ground state at small strain to an insulating state at large strain.[25] That is to say, with the increased strain, the Jahn–Teller distortion drives the double-exchange-induced metallic state gradually to become a charge-ordered insulating state. Therefore, the suppressed ferromagnetic metallic phase and the activation of the charge-ordered insulating state under the mechanical strain promote this huge resistivity change. If the flat state with low resistivity is set as the "on" state, the bending state with large resistivity is set as the "off" state. The resistivity change shows the huge change from the metal state to the insulator state in the LCMO thin films through the mechanical bending. High sensitivity makes our designed LCMO thin films promising for application in flexible resistivity switches at low temperature.

In conclusion, flexible epitaxial (111)-oriented LCMO thin films with STO buffer layers were fabricated on the F-Mica substrate using a pulsed laser deposition system. Both extra tensile and compressive mechanical strains make the MIT peaks of LCMO become subtle, and the transition temperature turns to lower temperature. Although the applied magnetic field provides energy to excite the charge carrier hopping and increases the MIT temperature, the energy is still not enough to overcome electron localization, and thus, the film exhibits insulator behavior at low temperature. The resistivity change by extra strain can go up to at least $10^5\%$ relative to that of no extra strain at 50 K since Jahn–Teller distortion tends to be enhanced by the extra mechanical tensile or compressive strain in the LCMO thin film. This huge resistivity change at low temperature suggests that the designed flexible LCMO thin film can be used as a bending-induced resistivity switch at low temperature.

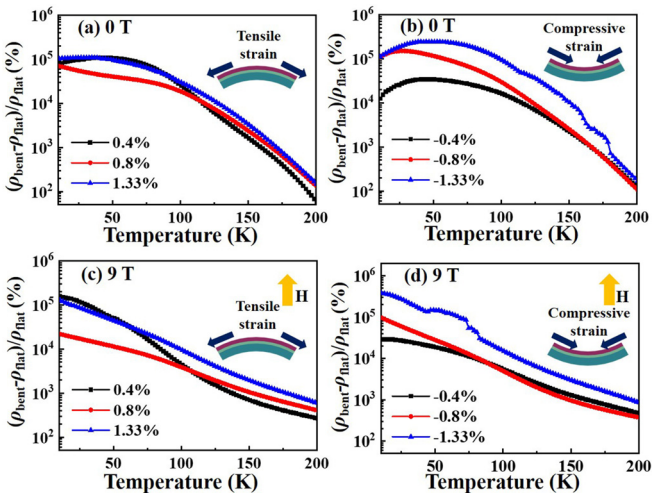

FIG. 4. Resistivity change ratio between the LCMO thin films under tensile and compressive strain and no extra strain at 0 T (a) and (b) and 9 T (c) and (d).

See the supplementary material for the bending strain calculation, details of transport properties under mechanical tensile and compressive strain in the linear coordinate system, and the thermal activation and small-polaron hopping model data fitting.

This research was supported by the Natural Science Foundation of China (Nos. 51702255 and 51390472), the National "973" projects of China (Nos. 2015CB654903 and 2015CB654603), Shaanxi Natural Science Foundation No. 2019JM-068, and the Fundamental Research Funds for the Central Universities.

DATA AVAILABILITY

The data that support the findings of this study are available from the corresponding author upon reasonable request.

REFERENCES

[1]S. Jin, T. H. Tiefel, M. McCormack, R. A. Fastnacht, R. Ramesh, and L. H. Chen, Science **264**, 413–415 (1994).
[2]R. von Helmolt, J. Wecker, B. Holzapfel, L. Schultz, and K. Samwer, Phys. Rev. Lett. **71**, 2331–2334 (1993).
[3]M. A. Subramanian, B. H. Toby, A. P. Ramirez, W. J. Marshall, A. W. Sleight, and G. H. Kwei, Science **273**, 81–84 (1996).
[4]A. S. McLeod, J. Zhang, M. Q. Gu, F. Jin, G. Zhang, K. W. Post, X. G. Zhao, A. J. Millis, W. B. Wu, J. M. Rondinelli *et al.*, Nat. Mater. **19**, 397–404 (2020).
[5]Y. Lu, X. W. Li, G. Q. Gong, X. Gang, G. Xiao *et al.*, Phys. Rev. B **54**, R8357 (1996).
[6]T. Sun, J. Jiang, Q. M. Chen, and X. Liu, Ceram. Int. **44**, 9865–9874 (2018).
[7]M. Viret, J. Nassar, M. Drouer, J. Contour, C. Fermon, and A. Fert, J. Magn. Magn. Mater. **198-199**, 1–5 (1999).
[8]Z. Guo, D. Lan, L. L. Qu, K. X. Zhang, F. Jin, B. B. Chen, S. W. Jin, G. Y. Gao, F. Chen, L. F. Wang *et al.*, Appl. Phys. Lett. **113**, 231601 (2018).
[9]K. Das and I. Das, J. Appl. Phys. **121**, 103904 (2017).
[10]M. Fath, S. Freisem, A. A. Menovsky, Y. Tomioks, J. Aarts, and J. A. Mydosh, Science **285**, 1540–1542 (1999).
[11]W. W. Gao, F. X. Hu, B. G. Shen, and J. R. Sun, J. Appl. Phys. **117**, 17C733 (2015).
[12]M. Navasery, S. A. Halim, A. Dehzangi, N. Soltani, G. Bahmanrokh, M. Erfani H, A. Kanalianfar, K. Y. Pan, S. C. Chang, S. K. Chen *et al.*, Appl. Phys. A **116**, 1661–1668 (2014).
[13]K. Kawashima, G. Logvenov, G. Christiani, and H. U. Habermeier, J. Magn. Magn. Mater. **378**, 539–545 (2015).
[14]B. B. Chen, P. F. Chen, H. R. Xu, X. L. Tan, F. Jin, Z. Guo, B. W. Zhi, and W. B. Wu, Appl. Phys. Lett. **104**, 242416 (2014).
[15]S. Das, A. Herklotz, E. J. Guo, and K. Dorr, J. Appl. Phys. **115**(14), 143902 (2014).
[16]Y. Li, J. R. Sun, J. Zhang, and B. G. Shen, J. Appl. Phys. **116**(4), 043916 (2014).
[17]S. E. Helali, K. Daoudi, A. Fouzri, M. Oumezzine, M. Oueslati, and T. Tsuchiya, Appl. Phys. A **108**, 379–384 (2012).
[18]M. Bibes, L. I. Balcells, S. Valencia, S. Sena, B. Martinez, and J. Fontcuberta, J. Appl. Phys. **89**(11), 6686–6688 (2001).

[19]S. Valencia, L. I. Balcells, B. Martinez, and J. Fontcuberta, J. Appl. Phys. **93**(10), 8059–8061 (2003).
[20]H. Wang, L. Shen, T. Duan, C. Ma, C. Cao, C. Jiang, X. Lu, H. Sun, and M. Liu, ACS Appl. Mater. Interfaces **11**, 22677–22683 (2019).
[21]J. Huang, H. Wang, X. Sun, X. Zhang, and H. Wang, ACS Appl. Mater. Interfaces **10**, 42698–42705 (2018).
[22]S. S. Hong, M. Q. Gu, M. Verma, V. Harbola, B. Y. Wang, D. Lu, A. Vailionis, Y. Hikita, R. Pentcheva, J. M. Rondinelli *et al.*, Science **368**, 71–76 (2020).
[23]P. Mandal, B. Bandyopadhyay, and B. Ghosh, Phys. Rev. B **64**, 180405 (2001).
[24]S. Li, C. Wang, Q. Shen, and L. Zhang, Vacuum **164**, 312–318 (2019).
[25]C. Sen and E. Dagotto, Phys. Rev. B **102**, 035126 (2020).
[26]M. Viret, L. Ranno, and J. M. D. Coey, Phys. Rev. Lett. **75**, 3910–3913 (1997).
[27]S. B. Li, C. B. Wang, D. Q. Zhou, H. X. Liu, L. Li, Q. Shen, and L. M. Zhang, Ceram. Int. **44**, 550–555 (2018).
[28]P. K. Siwach, H. K. Singh, and O. N. Srivastava, J. Phys. **18**, 9783–9794 (2006).
[29]C. R. Ma, M. Liu, J. Liu, G. Collins, Y. M. Zhang, H. B. Wang, C. I. Chen, Y. Lin, J. He, J. C. Jiang *et al.*, ACS Appl. Mater. Interfaces **6**, 2540–2545 (2014).